energies

MDPI

Article

Investigating the Behaviour of Air–Water Upward and Downward Flows: Are You Seeing What I Am Seeing?

Mukhtar Abdulkadir [1,*], Olumayowa T. Kajero [2], Fawziyah O. Olarinoye [3], Dickson O. Udebhulu [4], Donglin Zhao [5], Aliyu M. Aliyu [6] and Abdelsalam Al-Sarkhi [7]

1 Department of Chemical Engineering, Federal University of Technology, Minna PMB 65, Nigeria
2 Department of Chemical and Process Engineering, University of Surrey, Guildford GU2 7XH, UK; ot.kajero@gmail.com
3 Department of Petroleum Engineering, African University of Science and Technology, Garki, Abuja PMB 681, Nigeria; folarinoye21@gmail.com
4 Department of Mines and Petroleum Engineering, University of Sao Paolo, São Paulo 05508-010, Brazil; odudebhulu@usp.br
5 Department of Chemical and Petroleum Engineering, School of Engineering, London South Bank University, 103 Borough Road, London SE1 0AA, UK; donglin.zhao@lsbu.ac.uk
6 Department of Engineering and Technology, School of Computing and Engineering, University of Huddersfield, Queensgate, Huddersfield HD1 3DH, UK; a.m.aliyu@hud.ac.uk
7 Mechanical Engineering Department, King Fahd University of Petroleum and Minerals, Dhahran 31261, Saudi Arabia; alsarkhi@kfupm.edu.sa
* Correspondence: mukhau@futminna.edu.ng

Abstract: Understanding the behaviour of gas–liquid flows in upward and downward pipe configurations in chemical, petroleum, and nuclear industries is vital when optimal design, operation, production, and safety are of paramount concern. Unfortunately, the information concerning the behaviour of such flows in large pipe diameters is rare. This article aims to bridge that gap by reporting air–water upward and downward flows in 127 mm internal diameter pipes using advanced conductance ring probes located at two measurement locations. The liquid and gas flow rates are 0.021 to 0.33 m/s and 3.52 to 16.1 m/s, correspondingly, covering churn and annular flows. To achieve the desired objectives, several parameters, probability density function (PDF), power spectral density (PSD), Slippage Number (S_N), drift velocity (U_{gd}), and distribution coefficient (C_0) were employed. The flow regimes encountered in the two pipe configurations were distinguished employing a flow regime map available in the literature and statistical analysis. The obtained results were supported by visual inspection. The comparison between the present study against reported studies reveals the same tendency for the measured experimental data. The Root Mean Square Error (RMSE) method within 4% was utilized in recommending the best void fraction prediction correlation for the downward and upward flows.

Keywords: air–water system; downward flow; upward flow; large-diameter; liquid fraction; conductance ring probes

Citation: Abdulkadir, M.; Kajero, O.T.; Olarinoye, F.O.; Udebhulu, D.O.; Zhao, D.; Aliyu, A.M.; Al-Sarkhi, A. Investigating the Behaviour of Air–Water Upward and Downward Flows: Are You Seeing What I Am Seeing? *Energies* **2021**, *14*, 7071. https://doi.org/10.3390/en14217071

Academic Editor: Marco Marengo

Received: 4 September 2021
Accepted: 22 October 2021
Published: 28 October 2021

1. Introduction

1.1. Gas–Liquid Upward Flow in Small and Large Pipe Diameters

Gas–liquid upward flow finds applied applications in chemical engineering for mass transfer, the petroleum sector for concomitant oil and natural gas transport and the energy sector for heat transfer [1]. Consequently, it is imperative to have a firm knowledge of the behaviour of gas–liquid flow, a vital variable for the precise design of oil and gas production systems. A significant amount of effort for many decades has been dedicated by many researchers to achieve a comprehensive understanding of the behaviour of gas–liquid upward flows. Unfortunately, many of the reported works on such flows focus on small internal diameter pipes.

A small internal diameter pipe according to [2–4] is 9–55 mm (Abdulkadir et al. [4]). Notwithstanding, progress in several industries, from heat exchangers to large internal diameter deepwater risers, require the need for the understanding of gas–liquid flows in large diameter pipes, where the flow behaviour, maybe, considerably dissimilar from that in small ones [4]. On the other hand, a large diameter pipe in line with [5–9] is a pipe with an internal diameter > 100 mm [4]. Consequently, more attention needs to be given to the downward gas–liquid flow in large diameter pipes as in the upward flow.

1.2. Downward Gas–Liquid Flow

Gas–liquid downward flow in large diameter pipes is widely applied to many engineering applications such as nuclear reactors, steam injection wells, enriched gas injection wells where liquid condenses with pressure increase and riser pipes from offshore production platforms to the sea floor [10,11]. The knowledge of these flows in nuclear reactors is necessary for the safety analysis on the loss of coolant accidents in these reactors and plays a vital role in pressure drops precise measurement during oil and gas production and transportation over long distances. According to Wang et al. [12,13], the appropriateness of using upward experimental data to predict the loss of coolant accidents in downward flow nuclear reactors is questionable. Consequently, none of the upward flow correlations developed specifically for upward flow can be used for downward flow.

1.3. Gas–Liquid Upward and Downward Flows

The nature of flow regimes and the liquid fraction distribution gotten from upward and downward flows are expected to be significantly dissimilar, which has been confirmed by the conclusions of [14,15]. They concluded that the liquid fraction is presumed to be affected by the flow direction, buoyancy, and gravity force. The liquid fraction is of significance in the establishment of the flow pattern; it is the fraction of the pipe's cross-sectional area filled by the liquid phase [16]. Its determination according, to Abdulkadir et al. [16], is of considerable value in a range of engineering applications like enhancing safety and performance in industrial systems such as nuclear reactors, petroleum, and biomedical processing systems.

According to Bouyahiaoui et al. [17], flow patterns and void fraction disparity between vertical upward and vertical downward air–water flows in 12.7 mm internal diameter pipes was investigated by [1]. They observed significant discrepancies in the presence of the bubbly and slug flow patterns for the vertical upward and vertical downward flows. They reported the absence of churn flow in the vertical downward flow. Bhagwat and Ghajar [1] concluded that the drift–flux correlations of upward flow can be realized for the downward flow by reversing the sign of the drift velocity.

After two years, [18] studied the local interfacial characteristics in upward and downward bubbly flows in 50.8 mm internal diameter pipes by utilizing a four-sensor optical probe in the measurement of local interfacial parameters, including void fraction, interfacial area concentration (IAC), bubble frequency, interfacial velocity, and Sauter mean diameter. They compared the radial profiles of these parameters in the downward flow against those in the upward flow. They concluded that the void fraction showed a core-peaked distribution for the downward flow at a low void fraction but showed a wall-peaked distribution for the upward flow.

Chalgeri and Jeong [19] conducted two-phase flow experiments and plotted flow pattern maps for the vertical upward and downward flows from the measured data sets. They utilized a high-speed camera to visualize the flows, while a void fraction analysis was carried out by means of the electrical impedance technique and digital image analysis. They identified four and seven dissimilar flow regimes for the vertical upward and downward flows, respectively.

Recently, Bouyahiaoui et al. [17] examined the comparisons and differences between upward and downward air–water churn flow in a 34 mm internal diameter pipe for two arrangements of vertical upward (51 cases) and downward (48 cases). They used some

conductance probes and pressure transducers to measure cross-sectional averaged void fraction time series and pressure drop along the pipe, respectively. They also attempted to explicitly understand how gravity could influence the behaviour of liquid structures existing in the flow. They used various parameters such as probability density function (PDF), distribution coefficient in the drift–flux model, structure velocity, slippage number (S_N), dimensionless pressure gradient to achieve the objectives of their work. They reported that in both orientations, the dimensionless pressure gradient and S_N showed a strong correlation with the mixture Froude number. They, nevertheless, observed some inconsistencies in PDFs and structure velocities of flow in the two arrangements.

A summary of reviewed papers concerning upward and downward flows check listing the pipe geometries and experimental flow conditions is shown in Table 1. The reviewed papers revealed that the current state of understanding of upward and downward flows is limited because they are mainly concerned with small diameter pipes. The emphasis on the research in large diameter pipes was necessitated by the realization that the models based on the data from the small diameter pipes do not satisfactorily reflect the flow scenario in larger pipes. In addition, the ability to correctly predict the gas–liquid flow in large diameter pipes is remarkably essential for pump systems and nuclear safety.

The upward flow correlations developed specifically for upward flow cannot be utilized for downward flow based on the fact that it may lead to precautious uncertainty design and operations.

Table 1. Data from experiments involving upward and downward flows.

Reference	Fluids	Pipe Diameter (mm)	Flow Direction	Measured Parameters
Golan and Stenning [20]	Air–water	38.1	Upward and downward flows	Flow pattern
Beggs [21]	Air–water	25.4, 38.1	Upward and downward flows	Gas velocity distribution, Film thickness and local drop distribution
Oshinowo and Charles [22]	Air–water	25.4	Upward and downward flows	Void fraction
Nguyen [23]	Air–water	45.5	Upward and downward flows	Void fraction and pressure drop
Mukherjee [24]	Air–kerosene, air–lube oil	38.1	Upward and downward flows	Void fraction and pressure drop
Clark and Flemmer [25]	Air–water	100	Upward and downward flows	Void fraction
Jiang [26]	Air–water	9.525	Upward and downward flows	Void fraction
Jiang and Rezkallah [27]	Air–water	9.525	Upward and downward flows	Void fraction
Sun et al. [28]	Air–water	50.8	Upward and downward flows	Void fraction and axial liquid velocity
Lee et al. [29]	Air–water	25.4, 50.8	Upward and downward flows	Void fraction
Bhagwat and Ghajar [1]	Air–water	12.7	Upward and downward flows	Void fraction

Table 1. *Cont.*

Reference	Fluids	Pipe Diameter (mm)	Flow Direction	Measured Parameters
Tian et al. [18]	Air–water	50.8	Upward and downward flows	Void fraction and interfacial area concentration
Chalgeri and Jeong [19]	Air–water	Rectangular channel: 760 × 66.6 × 2.35	Upward and downward flows	Void fraction and flow pattern map
Bouyahiaoui et al. [17]	Air–water	34	Upward and downward flows	Void fraction and pressure drop

To examine liquid fraction behaviour in upward and downward flows quantitatively in pipes with diameters applicable to the energy industry in more detail, an air–water liquid fraction data was gathered using advanced conductance probes in 127 mm internal diameter pipes. Thus, this work reveals the effect of flow direction, buoyancy force and gravity force on the behaviour of liquid fraction in the upward and downward flows.

2. Theoretical Development

Models Utilized in Gas–Liquid Flow

The three common types of gas–liquid flow models utilized in the energy sector are Empirical correlations, Homogeneous models, and Mechanistic models.

Empirical correlations are established on the curve fitting of experimental data and are usually deployed to a confined range of variables examined in experiments. Homogenous models depict the fluid properties with mixture properties and utilize the procedures for single-phase flow to handle a two-phase flow mixture.

The Mechanistic model, the drift–flux model, is one of the most realistic and reliable models for gas–liquid flow study (Abdulkadir et al. [30,31]). The model, according to [30], recognises the influences of non-uniform flow, void fraction profiles, including the local relative velocity between the liquid and gas phases.

3. Materials and Methods

The two-phase air–water experiments reported in this work were conducted in a large flow loop facility. The test sections in the upward and downward flows pipe arrangements are made of polyvinyl chloride (PVC). Visualisation part is made of polymethyl methacrylate (PMMA). The test section in upward arrangement is 11 m tall and is equipped with an advanced conductance ring probe to measure the time-varying liquid fraction. The probe is located at 8.4 m above the air–water mixer as shown in Figure 1, which corresponds to 66 pipe diameters above the air–water mixer region.

The air–water downward flow loop comprises three principal parts: an inverted 180° bend (bend radius/pipe diameter = 3), a 9.6 m long downward pipe with an advanced conductance ring probe fitted at about 21 pipe diameters from the bend; this is 2.667 m downstream of the bend and a 1.5 m long horizontal pipe to the separator.

The experimental flow facility shown in Figure 1 has been published earlier by several authors, namely, [4,6,32–37]. Hence specifics of the experimental facility are obtainable from the published articles. However, a concise description of the experimental facility is discussed below to improve the reader's comprehension. The facility works as follows:

Two large liquid ring-pump compressors actuated by two 55-kW motors were employed to provide air; it was metered by a calibrated vortex meter and supplied through a pipe base, thus facilitating its mixture with water collected from the liquid storage tank (which is also a phase separator). The mixed air–water system is then delivered by one of the turbine flow meters (both turbine flow meters are installed in parallel). The 4 m height, 1 m diameter, and 4 m^3 liquid storage cylindrical tank is high-grade stainless steel.

For the present experimental study, 1.6 m^3 of water was stored in the tank. According to Abdulkadir et al. [4], the maximum calculated uncertainties associated with the flow meters are ±0.5% and ±0.6% for the water and air, respectively.

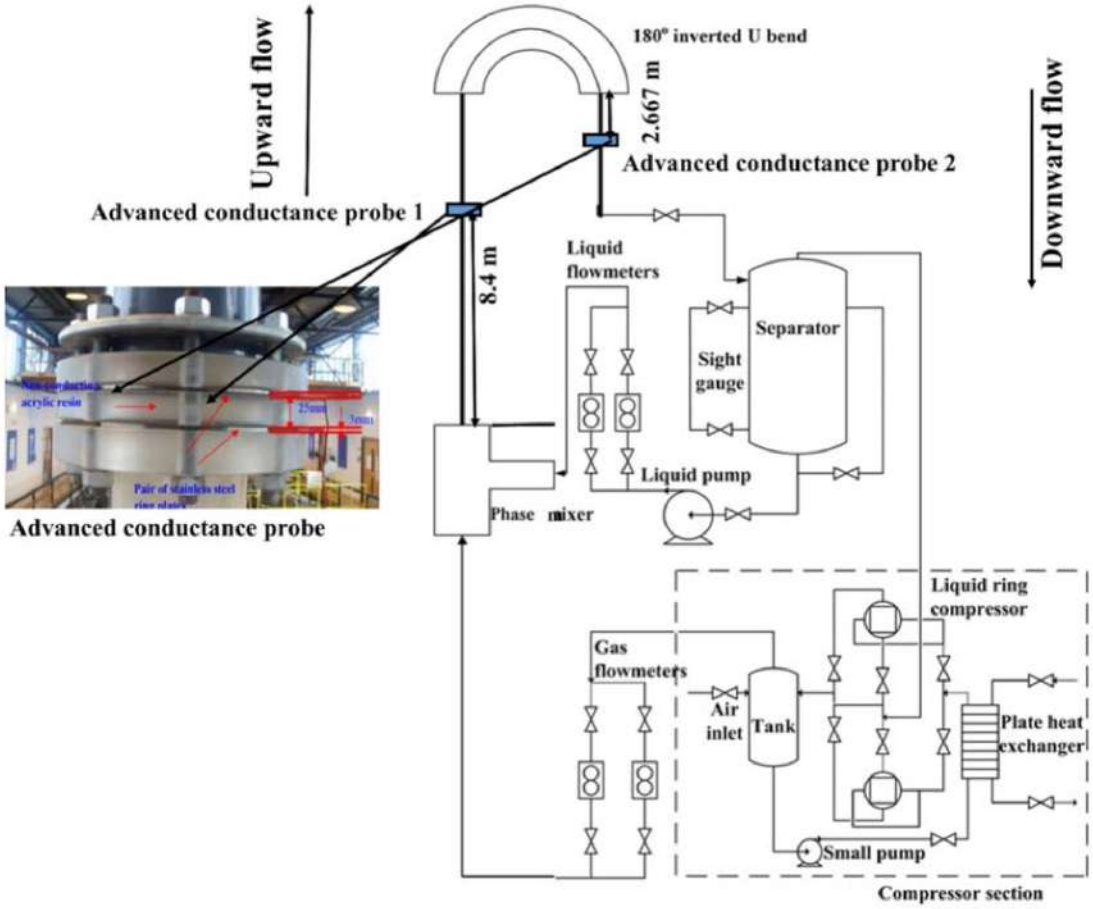

Figure 1. The diagrammatic representation of the experimental flow facility used in this study.

The air–water mixer, an annular injection mixing device, according to [16], is made of a 0.105 m diameter tube placed at the middle, concentric with the 0.127 m internal diameter test section. The hybrid air–water system is then flown through the upward pipe before getting to the inverted 180° bend [4].

The air and tap water mixture on reaching the bend and exiting it travels 9.6 m downwards, then 1.5 m in a horizontal direction to the separator, where the two phases (air–water system) are separated before the pump compressors are used to deliver the separated phases back [16].

The scope of the liquid and gas flow rates considered in this work are 0.021–0.33 m/s and 3.52–16.1 m/s, respectively. The measurements were obtained at the operating temperature and system pressure of 20 °C and 2 bar (gauge), respectively. The gauge pressure was used because the system pressure was greater than the local atmospheric pressure. It was set at 2 bar because the flow process was at 1 bar. The advanced conductance probes placed at the two pipe configurations were utilized to record time-varying liquid fraction data every 0.001 s for 15 s per experimental run. Each run was repeated three times to ensure reproducibility and replicability of data. Table 2 shows the air–water properties and the range of liquid fractions examined in this work.

Table 2. Fluid properties at the operating temperature of 20 °C and system pressure of 2 bar (gauge).

Fluid	Density (kg/m^3)	Viscosity (kg/ms)	Surface Tension (N/m)	Range of Liquid Fraction
Air	3.55	0.000018		0.02–0.11
Tap water	998.00	0.00089	0.072	

3.1. Instrumentation

3.1.1. Liquid Fraction Measurement Using the Omebere–Iyari's Conductance Ring Probes

Figure 2 shows the conductance ring probes used to obtain the liquid fraction data. The probes were designed carefully by Omebere-Iyari [32] to guarantee that the electrodes had an identical diameter, *D*, as the test section (127 mm) to ensure flush mounting with the pipe wall [4]. According to Abdulkadir et al. [4], [32] ensured that the distance between each pair of stainless-steel electrode plates, *De*, and width, *S*, shown in Figure 2, are 25 and 0.3 mm, respectively. The outcome is a *De/D* of 0.20 and *S/D* of 0.024. Omebere-Iyari [32] concluded that a liquid fraction/dimensionless conductance relationship was achieved by reproducing the method with plastic rods of various diameters. The reader is referred to [32] for more details.

Figure 2. Conductance ring probes (**a**) impression of the calibration set-up with the conductance probe rings (in red), a water portion (in blue) and the non-conducting cylinder (in grey) [6] (**b**) the parallel conductance ring probe [4].

Omebere–Iyari [32] simulated annular and churn flow patterns by placing a dielectric plastic rod in the pipe while the annulus between the pipe and the plastic rod was filled with a liquid that conducts [4]. Unfortunately, the [32]'s conductance ring probes failed to account for the gas bubbles within the liquid film. As a result, the utilization of the probes that can account for gas bubbles entrained within the liquid film became necessary.

3.1.2. Liquid Fraction Measurement Using the New Conductance Ring Probes

Van der Meulen et al. [33] adapted [32]'s method to account for the influence of gas bubbles entrained within the liquid film by simulating the gas bubbles entrained within the liquid film and then recalibrating the probes. They achieved this by occupying the region between the pipe wall and the non-conducting rod with an identified quantity of spherical glass beads of varying diameters, from 0.003 to 0.006 m [4]. The output of the conductance ring probes is proportional to the combined resistance of the air–water system varies from 0 to 0.32 V.

For this reason, the newly re-calibrated probes were designated in this present work as advanced conductance ring probes because they account for the influence of gas bubbles entrain within the liquid film. These re-calibrated probes have been utilized by several

researchers, including [4,6,16,34–37] among others. A personal computer equipped with a National Instrument data acquisition card was used to gather the liquid fraction data. It is worth mentioning that Van der Meulen [6] modified the [32]'s developed data retrieval program in LabVIEW represented by a third-order polynomial fit:

$$\text{Liquid fraction} = h + e(Ge^*) + f(Ge^*)^2 + g(Ge^*)^3 \quad (1)$$

where: Ge^* is the normalised voltage response of the probe.

Equation (1) was utilized to obtain the characteristic calibration curve applied for the individual probes. The calibration curves of [32,33], covering the range of liquid fractions in the present study, are presented in Figure 3. The reader is referred to Van der Meulen [6] for additional information on the re-calibrated probes (calibration with the glass beads). To improve measurement accuracy and in line with Fossa [38], the conductance ring probes used in the presented work were recalibrated.

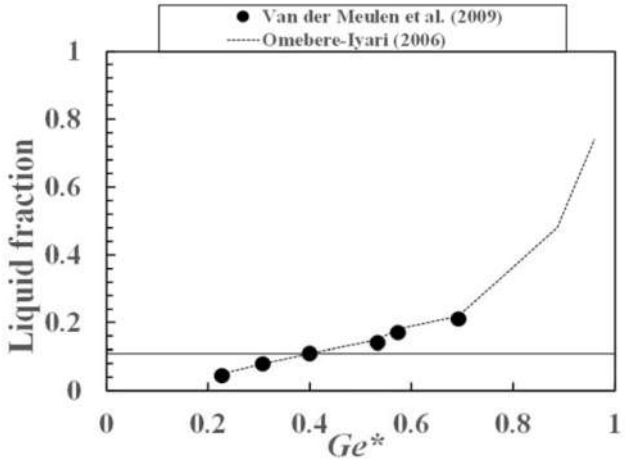

Figure 3. Calibration curves for the conductance ring probes by [32,33] covering the range of liquid fraction in the present study.

4. Results and Discussion

The liquid and gas volumetric flow rates shown in Table 3 are the operating parameters used in this study. An entire 170 liquid fraction data were acquired for the downward and upward flows conditions throughout the experimental campaigns.

Table 3. The scope covering the measured variables.

Air Superficial Velocity, U_{SG} (m/s)	Water Superficial Velocity, U_{SL} (m/s)
3.52–16.1	0.021–0.33

4.1. Flow Regime Map

Figure 4 graphically displays on the Pereyra and Torres [39]'s flow regime map of the 85 upward flow experimental data points from this work. On the other hand, the 85 downward flow data points are presented in Figure 5. From the [39] flow regime map, annular and churn flows are noticed in the upward flow arrangement, while only annular flow is observed in the downward flow arrangement. The transition lines presented in Figure 4 were obtained by employing the mechanistic equations proposed by Taitel et al. [40] model for bubble/slug flow transition; [39] model for churn/annular flow transition; and the Jayanti and Hewitt [41] model for slug/churn flow transition. Therefore, it can be concluded that the proposed [39] model for the churn/annular flow transition is inaccurate and appears to under-predict the annular flow conditions examined. On the contrary, Figure 5 shows that only annular flow is predicted for the downward flow conditions.

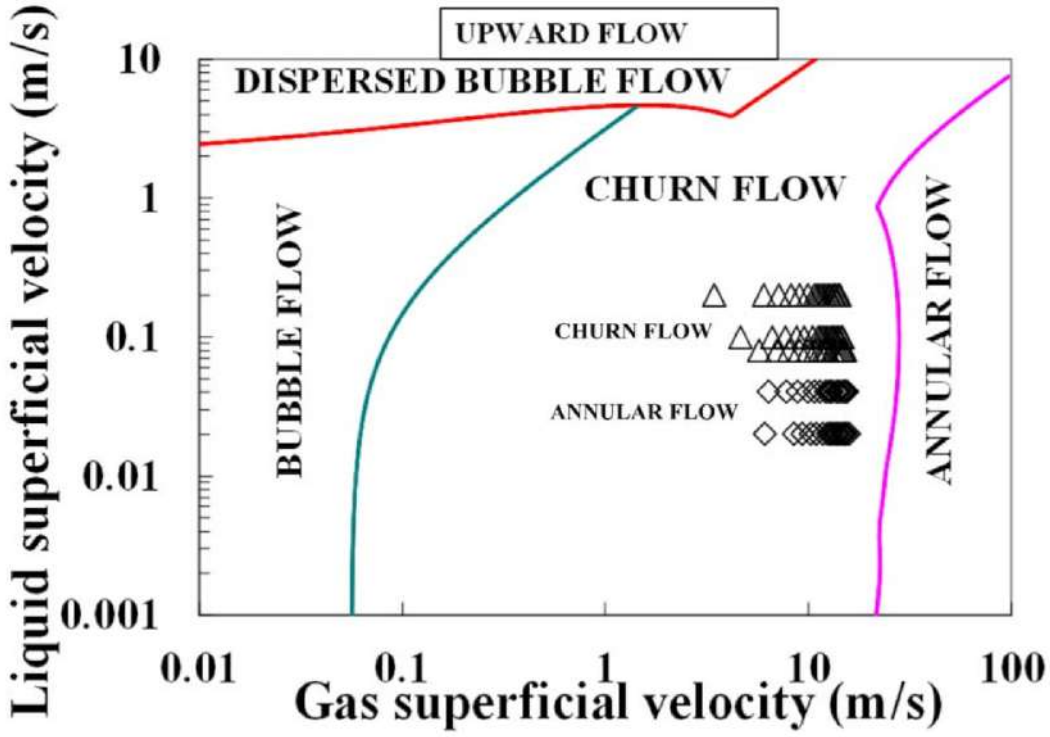

Figure 4. The Pereyra and Torres [39] flow regime map displaying the locations of experimental points of study encountered in upward flow utilising air–water as the system fluid. The transition lines are based on the previous predictions while the symbols represent present experimental data.

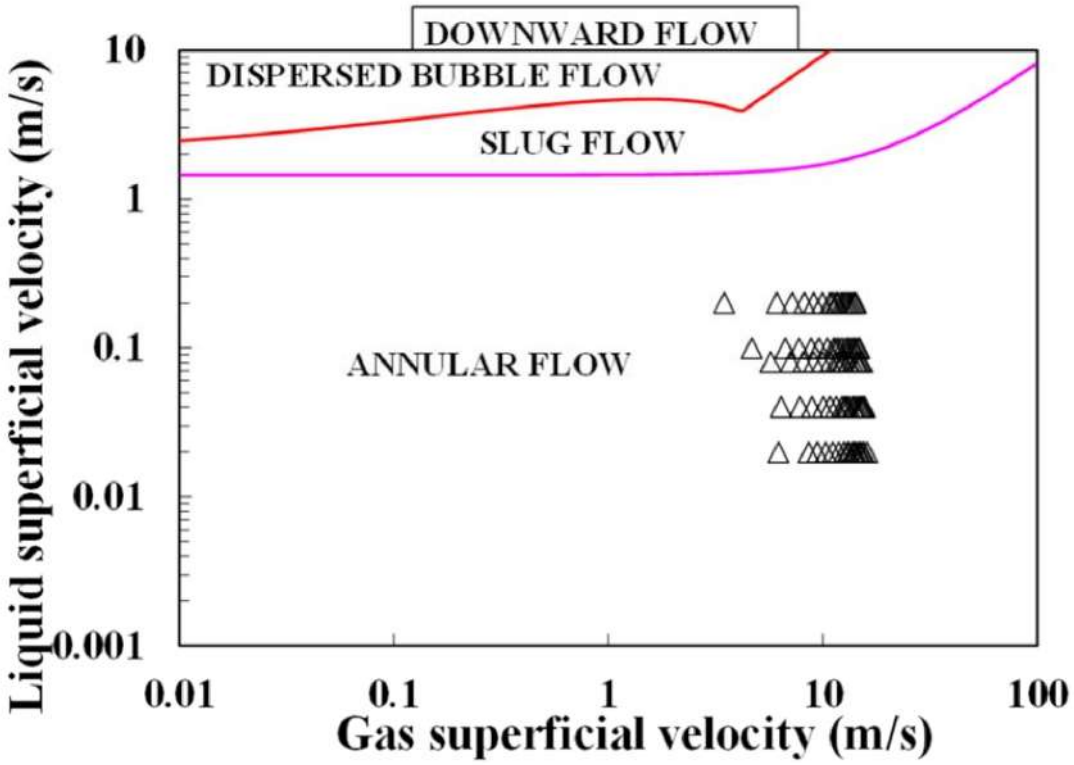

Figure 5. The Pereyra and Torres [39] flow regime map displaying the locations of experimental points of study encountered in downward flow utilising air–water as the system fluid. The transition lines are based on the previous predictions while the symbols represent present experimental data.

4.2. The Accuracy of the Conductance Ring Probes

Omebere–Iyari [32] has previously provided a comprehensive explanation of the conductance ring probes' design. The reproducibility of the calibration and measurement procedures was a priority in this study. It is important to mention that the uncertainty in liquid fraction measurement using absolute error, according to Abdulkadir et al. [16], was found to range from 0.018 to 0.027 for all measurements taken; this corresponds to a range of 1.8% to 5% relative error.

4.2.1. Comparing this Study Approach with Those of Godbole et al. and Bhagwat and Ghajar

The average void fraction for the upward and downward flows gotten from the present work is compared against the [42] and Bhagwat and Ghajar [1] data. Both [42] and [1] employed the same experimental rig (pipe with an internal diameter of 0.0127 m), working fluid (air and water) and quick closing valve technique to gather void fraction data. It is interesting to note that the pipe employed in the present work is ten times bigger than that of the pipes employed by both.

The upward flow comparison is based on present work against the experimental void fraction data of [42] at the same gas and liquid superficial velocities of 4.64–4.8 m/s and 0.1 m/s, respectively. The outcome of this comparison are presented in Figure 6. However, for the downward flow direction, this present work will be compared against the [1] experimental void fraction data at the same gas and liquid superficial velocities of 5.72–15.2 m/s and 0.08 m/s, respectively. Figure 7 shows the results of the comparison.

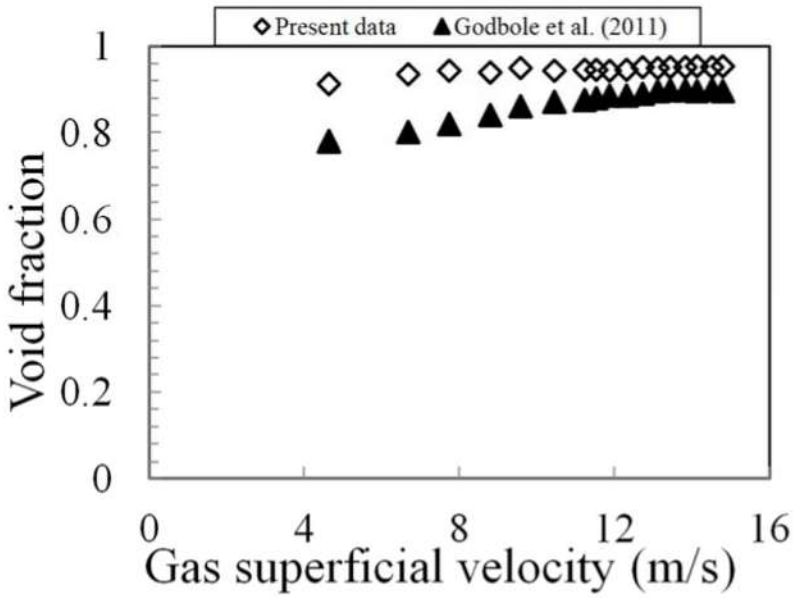

Figure 6. Comparing present experimental void fraction data against the experimental data of Godbole et al. [42] for upward flow at the same gas and liquid superficial velocities of 4.64–4.8 m/s and 0.1 m/s, respectively. The absolute errors are between 0.018 and 0.027, this corresponds to 1.8% to 5% relative error for most of the data.

Figure 6 reveals that the void fraction from the present work exhibits the same tendency as the [42]'s experimental data, though the values of the void fraction obtained from [42] are lower. The observed trend maybe because the quantity of drops of liquid entrained in the gas matrix is lower in the smaller diameter pipe than in the larger diameter one, leading to a higher observed void fraction in the large-diameter pipe. Similarly, the values of void fraction obtained from [1] work, as shown in Figure 7, are also lower than those of the present work.

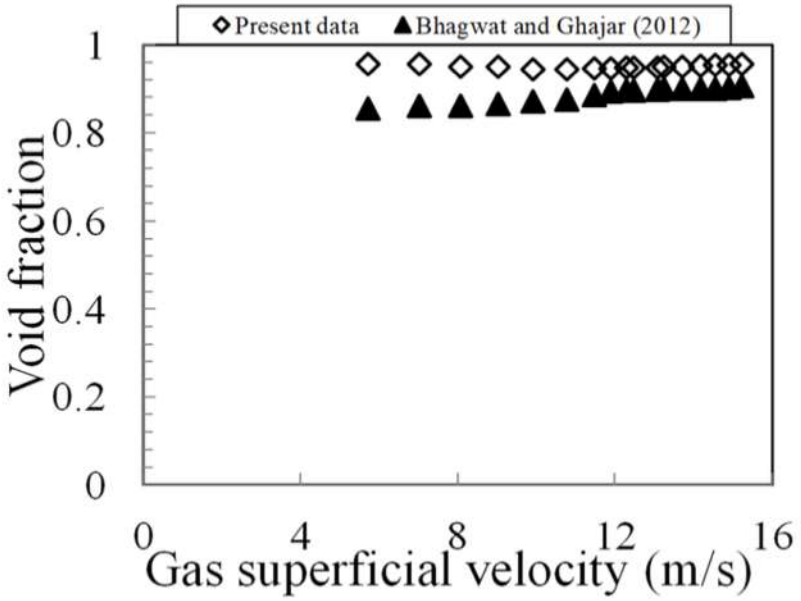

Figure 7. Comparing this study's void fraction experimental data against the experimental data of Bhagwat and Ghajar [1] for downward flow at the same gas and liquid superficial velocities of 5.72–15.2 m/s and 0.08 m/s, respectively.

4.2.2. Comparison between Present Study and That of Zangana and Abdulkadir et al.

The comparison between the current work and that of Zangana [34] and Abdulkadir et al. [4] will be carried out at the same liquid and gas superficial velocities of 0.33 and 6.2–14.2 m/s, respectively, using average liquid fraction data. The current work employed the same experimental rig utilized by [4,35] to carry out their experimental work. However, [4,34] and the present study placed their measuring instruments at 8.2, 8.3, and 8.4 m, respectively.

The outcome of the comparison is shown in Figure 8. Although with some insignificant variations, the graph displays the similar trend at some gas superficial velocities. The observed variations might be because the measurement stations are not the same.

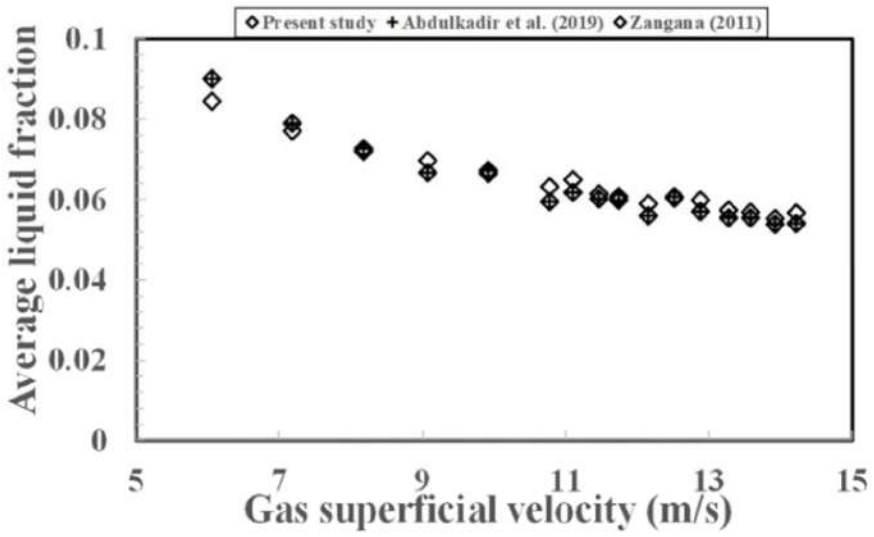

Figure 8. A comparison between the present study and those of Zangana [34] and Abdulkadir et al. [4]. Liquid and gas superficial velocities of 0.33 and 6.2–14.2 m/s, respectively. System fluid: air–water. Pipe internal diameter (mm): 127.

4.3. Typical Time Varying, Liquid Fraction and Liquid Film Thickness, Power Spectral Density (PSD), and Probability Density Function (PDF) Plots for Downward and Upward Flows

Figure 9 shows a typical time series plot of liquid fraction, PSD, and PDF of liquid fraction for the downward and upward flows at gas and liquid superficial velocities of 9.9 m/s and 0.08 m/s, respectively.

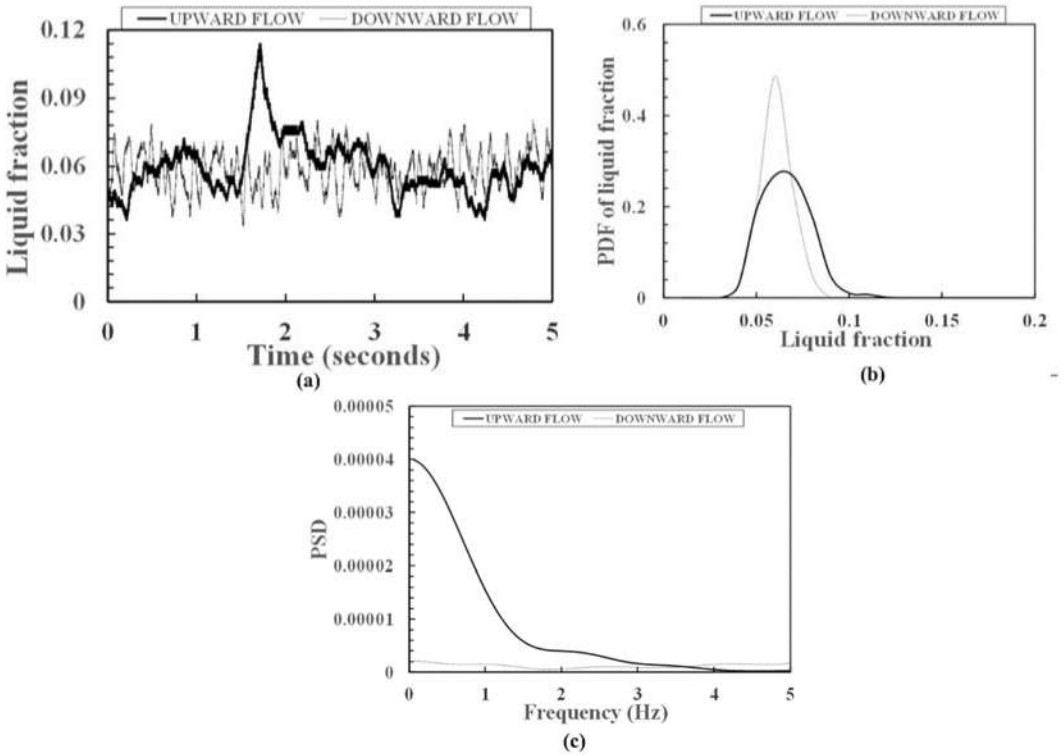

Figure 9. (**a**) Time-varying liquid fraction (**b**) PDF of liquid fraction and (**c**) PSD of liquid fraction for the downward and upward flows.

(a) Time series of liquid fraction for the downward and upward flows:

An investigation of the time trace of liquid fraction for the upward flow suggests that the ensuing flow regime is churn flow. It is churn flow because the time series plot shows that the average liquid fraction is 0.0638 (void fraction = 0.9362). Figure 10 shows based on the liquid film thickness plot that the liquid film is irregular and shows significant disturbances with liquid film thickness up to or greater than 0.10.

These disturbances, otherwise called waves acting on the liquid fraction or liquid film thickness time trace, are created because of the enormous gas shear stress exerting the gas–liquid interface. Visual inspection was used to confirm the presence of the waves. In this work, the Equation (10) that was employed to determine the individual liquid film thickness was derived from the average cross-sectional liquid fraction as follows with the assumption that the liquid film is symmetrical about the pipe axis.

From

$$\varepsilon_G = \frac{A_g}{A_g + A_l} = \frac{A_g}{A} \tag{2}$$

$$A_g = \pi d_{core}^2/4 \tag{3}$$

$$A = \pi D^2/4 \tag{4}$$

Derived from Figure 11, $D = d_{core} + 2\delta$.

where δ, d_{core}, and D, represents the liquid film thickness, diameter of the gas core and the pipe internal diameter, respectively.

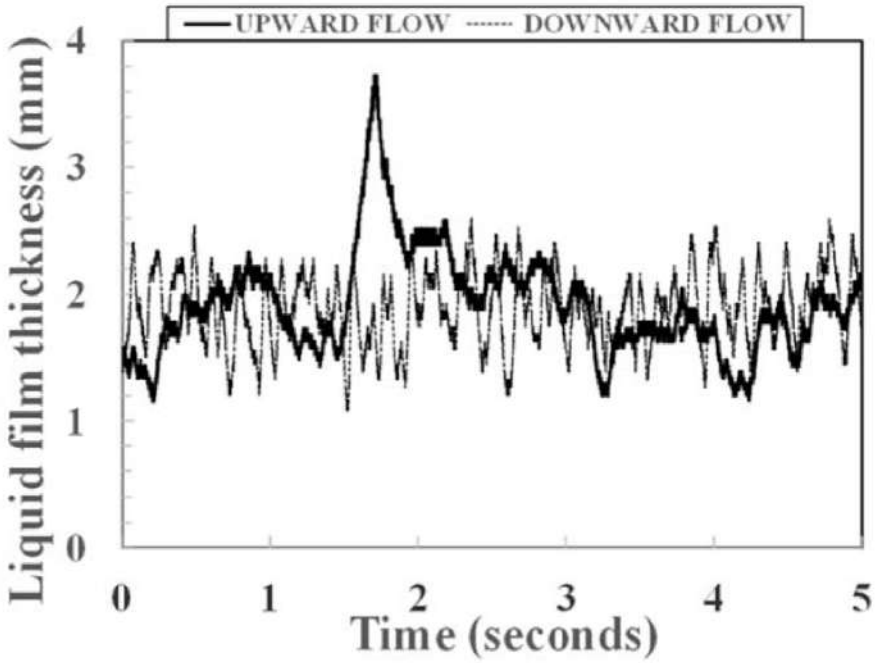

Figure 10. Typical time-varying liquid film thickness for the downward and upward flows.

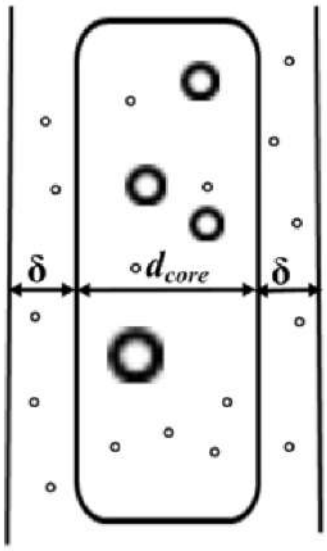

Figure 11. Diagram of a typical annular flow showing some droplets of liquid in the gas matrix (core) and in the liquid film region.

Thus,

$$d_{core} = D - 2\delta \tag{5}$$

Substituting Equation (5) into (3)

$$A_g = \pi(D - 2\delta)^2/4 \tag{6}$$

Substituting Equations (4) and (6) into (2)

$$\varepsilon_G = \pi(D - 2\delta)^2/4 \times 4/\pi D^2 \tag{7}$$

$$\varepsilon_G = ((D - 2\delta)/D)^2 \tag{8}$$

$$\sqrt{\varepsilon_G} = \left(\frac{D}{D}\right) - \left(\frac{2\delta}{D}\right) = 1 - \frac{2\delta}{D}$$

$$\delta = \frac{D}{2}[1 - \sqrt{\varepsilon_G}] \tag{9}$$

Substituting the void fraction, ε_G, with liquid fraction, ε_F, and bearing in mind that $\varepsilon_G = 1 - \varepsilon_F$.

Therefore,

$$\delta = \frac{D}{2}\left[1 - \sqrt{(1 - \varepsilon_F)}\right] \tag{10}$$

When the direction of flow is downwards, the gas moves towards the pipe centre while the liquid travels to the pipe walls. The observed behaviour can be associated with the fact that both flow and gravity act in the same (downward) path for the liquid, whereas for the gas, buoyancy force plays in the opposing (upward) path; thus, the flow regime changes to annular flow. In addition, the flow pattern, according to Figure 9a, is annular for the downward flow because the liquid fractions from the time series are continually below 0.07 with very slight disturbances compared to those seen in churn flow.

(b) Probability density function (PDF) of liquid film fraction for the upward and downward flows:

The PDF is employed in this work as shown in Figure 9b to reveal the dominant liquid fraction observed for every flow condition. The figure shows that the flow regime is churn flow for the upward flow. It is churn flow because the PDF plot depicts a single crest at a low liquid fraction of 0.07, but with a broad base stretching at liquid fractions of 0.03 and 0.12. This is in line with the observation of Costigan and Whalley [43]. In contrast, the flow pattern is annular for the downward flow because the PDF depicts a single crest at a low liquid fraction with a narrow base.

(c) Power spectral density (PSD) against frequency:

The PSD analysis shown in Figure 9c was carried out in this work to remove the subjectivity inherent in frequency determination. The figure shows how the PSD varies with frequency for the downward and upward flows at gas and liquid superficial velocities of 9.9 m/s and 0.08 m/s, respectively. The PSD plot according to Figure 9c for the upward flow contains a crest at about zero frequency. According to Abdulkadir et al. [4], this kind of response is associated with churn flow. In contrast, the PSD plot possesses a flat and relatively uniform spectrum akin to annular flow for the downward flow.

4.4. The Effect of Flow Direction, Buoyancy, and Gravity Forces on the Average Liquid Fraction

This section aims to interrogate the influence of flow direction, buoyancy, and gravity forces on the liquid fraction behaviour. The average liquid fraction obtained from the upward flow is matched against that from the downward flow scenario under the same flow conditions to achieve this aim. Figure 12a–d, therefore, reveals the effect of flow direction, buoyancy, and gravity forces on liquid film and how the average liquid fraction at various liquid superficial velocities varies with the gas superficial velocity.

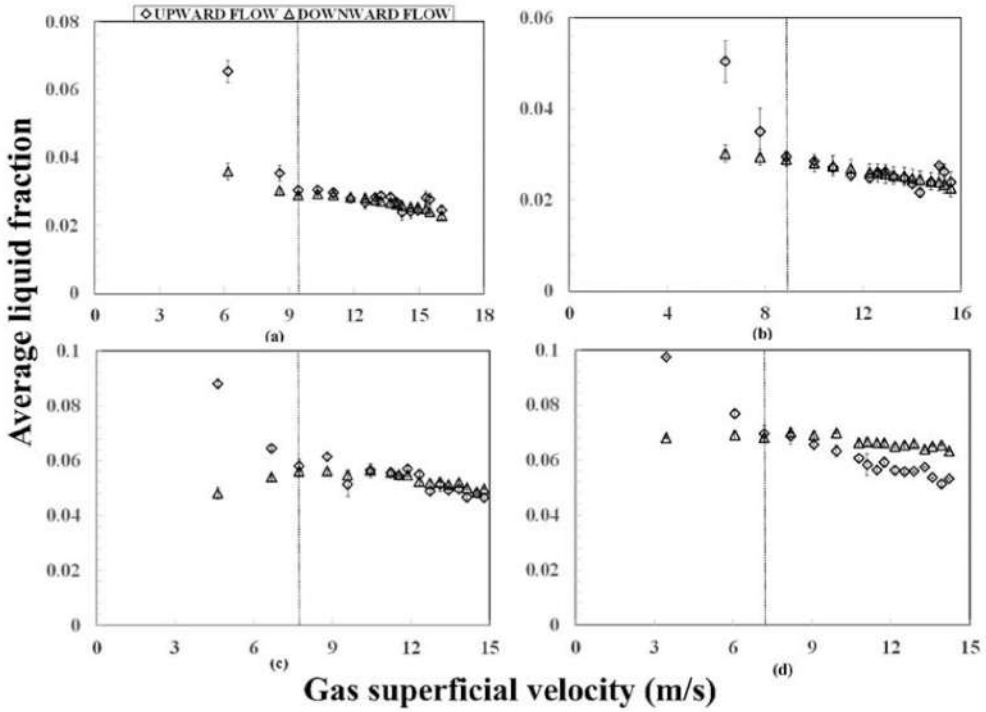

Figure 12. The effect of flow direction, buoyancy, and gravity forces on average liquid fraction for the downward and upward flows at liquid superficial velocity of: (**a**) 0.02 m/s, (**b**) 0.04 m/s, (**c**) 0.1 m/s, and (**d**) 0.2.m/s. The standard deviation is indicated by the error bar.

The figure shows that the liquid fraction for the upward and downward flows reduce with increasing gas superficial velocity. The observed trend could be as a result of an increase in gas production leading to a corresponding decrease in liquid fraction as the gas superficial velocity increases. Although, the observed liquid fractions at lower gas superficial velocities are significantly lower for the downward flow than the upward flow scenario. This behaviour is not surprising because in the upward flow, the gas phase's buoyant force supports the flow direction while the gravity force plays in the opposite direction. On the other hand, the gravity force and flow direction counteract the gas phase's buoyant force in the downward flow. As a result, higher liquid fractions are seen for the upward flow due to a decrease in the gas phase volume because of the tendency of the gas to more swiftly than the liquid in comparison to the downward flow scenario, for the same liquid and gas superficial velocities. The disparity in the liquid fractions' values for the downward and upward flows decreases with an increase in the gas superficial velocity.

4.5. Correlation of Slippage Number (S_N) with Mixture Froude Number (FrM)

The relationship between the Slippage Number (S_N) and Mixture Froude Number (FrM) at various liquid superficial velocities is shown in Figure 13.

S_N, a dimensionless number, according to Al-Sarkhi et al. [44] is a function of ρ_m, ε_G, ρ_H, and λ_L, and is defined as the ratio of the difference in the gravitational forces between the slip and no-slip conditions to the inertial force of the gas. Mathematically,

$$S_N = \frac{(\rho_m - \rho_H)Dg}{\rho_G U_{SG}^2} \tag{11}$$

where,

$$\rho_m = \rho_G \varepsilon_G + \rho_L \epsilon_F \tag{12}$$

$$\rho_H = \rho_G(1 - \lambda_L) + \rho_L \lambda_L \tag{13}$$

$$\lambda_L = \frac{U_{SL}}{U_m} = \frac{U_{SL}}{U_{SL} + U_{SG}} \tag{14}$$

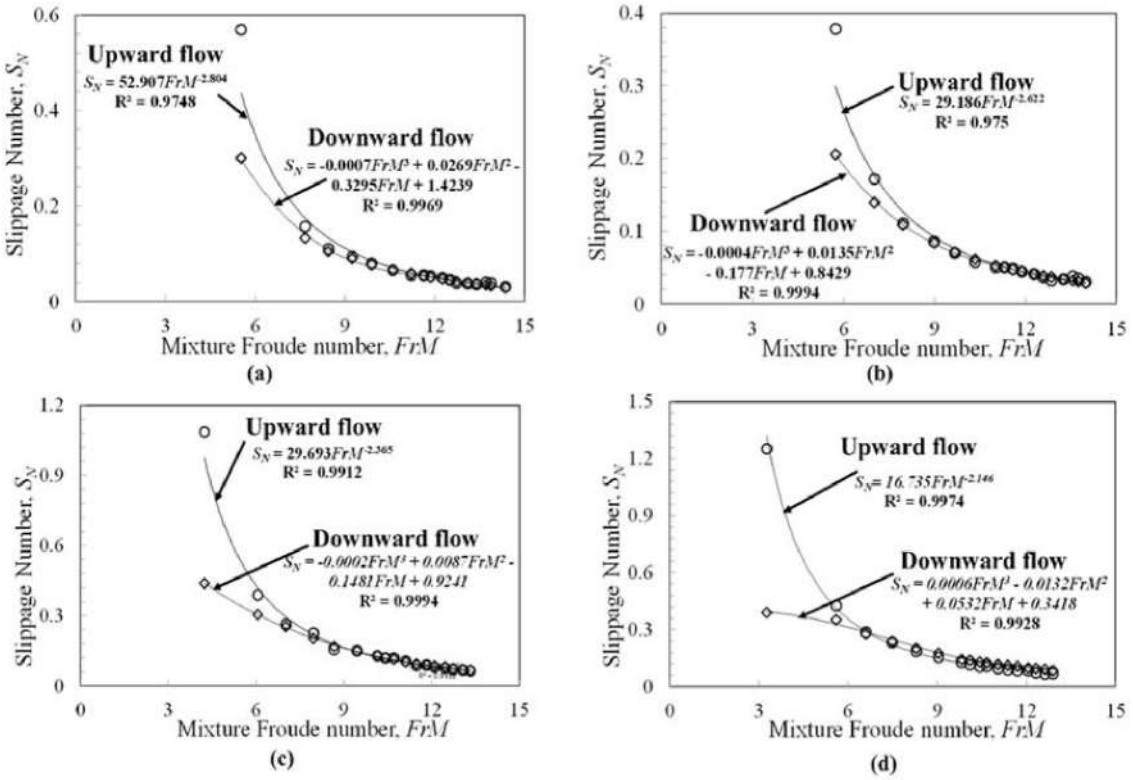

Figure 13. Correlation of Slippage Number (S_N) with mixture Froude number (FrM) for the upward and downward flows. System fluid: air–water. Flow pattern under consideration: Churn and annular flows. Liquid superficial velocity of (**a**) 0.021 m/s (**b**) 0.04 m/s (**c**) 0.1 m/s and (**d**) 0.2 m/s.

S_N is plotted in the current work versus the mixture Froude number, FrM. The Froude number is a non-dimensional number that describes the ratio of the inertial forces to the gravity forces. According to [44], FrM is explained mathematically as:

$$FrM = \sqrt{\frac{\rho_L}{(\rho_G + \rho_L)}} \frac{U_m}{\sqrt{gD}} \tag{15}$$

when $U_{SL} \ll U_{SG}$, U_m (=U_{SL} + U_{SG}) $\approx U_{SG}$, FrM is replaced with Fr_{SG} and hence, Equation (15) becomes:

$$Fr_{SG} = \sqrt{\frac{\rho_L}{\rho_G + \rho_L}} \frac{U_{SG}}{\sqrt{gD}} \tag{16}$$

Figure 13 establishes that for either the upward or downward flow, S_N decreases as FrM increases as it has been reported in the literature by [17] for upward and downward flows and [44] for upward flows. The decrease in the values of S_N due to increases in the values of FrM can be attributed to a drop in the slippage between the two phases and the difference between the local two-phase flow mixture density and the homogeneous mixture density. Though, there is a very good correlation between S_N and FrM for all the liquid superficial velocities considered. Equations (17)–(24) are the correlations obtained by curve fitting of the plots in Figure 13a–d for the range of liquid superficial velocity investigated (0.02–0.2 m/s) for the upward flow. The graph of S_N versus FrM for the downward flow data displayed on the same graph also exhibits a perfect match.

$$S_N = 52.907 Fr_M^{-2.804} \tag{17}$$

$$S_N = 0.0007Fr_M^3 + 0.0269Fr_M^2 - 0.3295Fr_M + 1.4239 \quad (18)$$

$$S_N = 29.186Fr_M^{-2.622} \quad (19)$$

$$S_N = -0.0004Fr_M^3 + 0.0135Fr_M^2 - 0.177Fr_M + 0.8429 \quad (20)$$

$$S_N = 29.693Fr_M^{-2.365} \quad (21)$$

$$S_N = -0.0002Fr_M^3 + 0.0087Fr_M^2 - 0.1481Fr_M + 0.9241 \quad (22)$$

$$S_N = 16.735Fr_M^{-2.146} \quad (23)$$

$$S_N = 0.0006Fr_M^3 - 0.0132Fr_M^2 + 0.0532Fr_M + 0.3418 \quad (24)$$

The figure shows that for larger *FrM*, the values of S_N for the upward and downward flows are nearly identical. This demonstrates that the liquid and gas flow together as a homogeneous mixture. Furthermore, the values of S_N changes from the least for annular flow (Figure 13a,b) to the highest for churn flow (Figure 13c,d). This is so because the gas superficial velocities encountered in annular flow are moderately greater than those in churn flow, and as expected, the slippage between the gas and liquid is lower than that in churn flow. As a result, the difference between the local two-phase flow mixture density and the homogeneous mixture density, in addition to S_N, are lower in annular flow compared to those in churn flow.

A closer look at Equation (15) shows that when U_{SG} is dominating, the *x*-axis becomes approximately U_{SG}, as shown in Equation (16). A test of this assumption was obtained by making a plot of S_N against Fr_{SG}. It is important to mention that for the upward flow, U_{SG}/U_m and void fraction values are in the ranges of 0.95–1.0 and 0.95–0.98, respectively. Conversely, for the downward flow, values of U_{SG}/U_m and void fraction are in the ranges of 0.95–1.0 and 0.93–0.98, respectively.

A conclusion can be drawn, therefore, based on Figure 14 that the assumption made earlier that U_{SG} is approximately equal to U_m holds because the values of U_{SG}/U_m are indeed approximately equal to 1.0. Furthermore, it is strengthened by the obtained range of values of void fraction, 0.95–0.98 and 0.93–0.98, for the upward and downward flows, respectively.

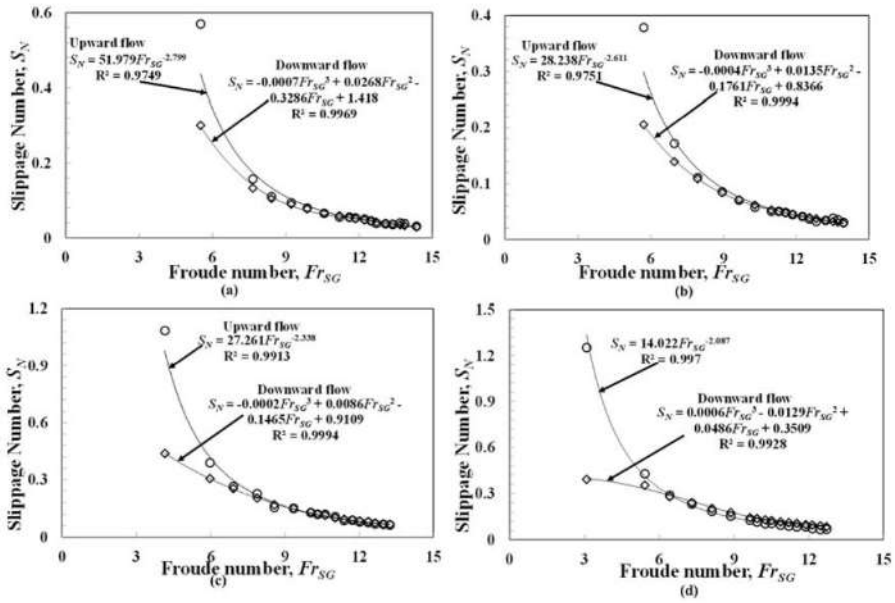

Figure 14. Relationship between Slippage Number (S_N) and Froude Number (Fr_{SG}) for the upward and downward flows. System fluid: air–water. Flow pattern under consideration: Churn and annular flows. Liquid superficial velocity of (**a**) 0.02 m/s (**b**) 0.04 m/s (**c**) 0.1 m/s and (**d**) 0.2 m/s.

To further test the validity of assuming U_{SG} to be approximately equal to U_m, the experimental data of Abdulkadir et al. [31] for an air–silicone oil system flowing in a vertical pipe whose internal diameter pipe is 67 mm was used. Silicone oil is a liquid whose viscosity is five times the viscosity of water. The gathered data were sorted into the prevailing flow patterns and plotted, as shown in Figures 15 and 16. With the former representing slug flow and the latter, churn flow. The range of values of U_{SG}/U_m and void fraction for the slug flow regime are 0.43–0.95 and 0.27–0.59, respectively, whereas, for churn flow, the values of U_{SG}/U_m and void fraction are in the range of 0.79–0.99 and 0.59–0.90, respectively.

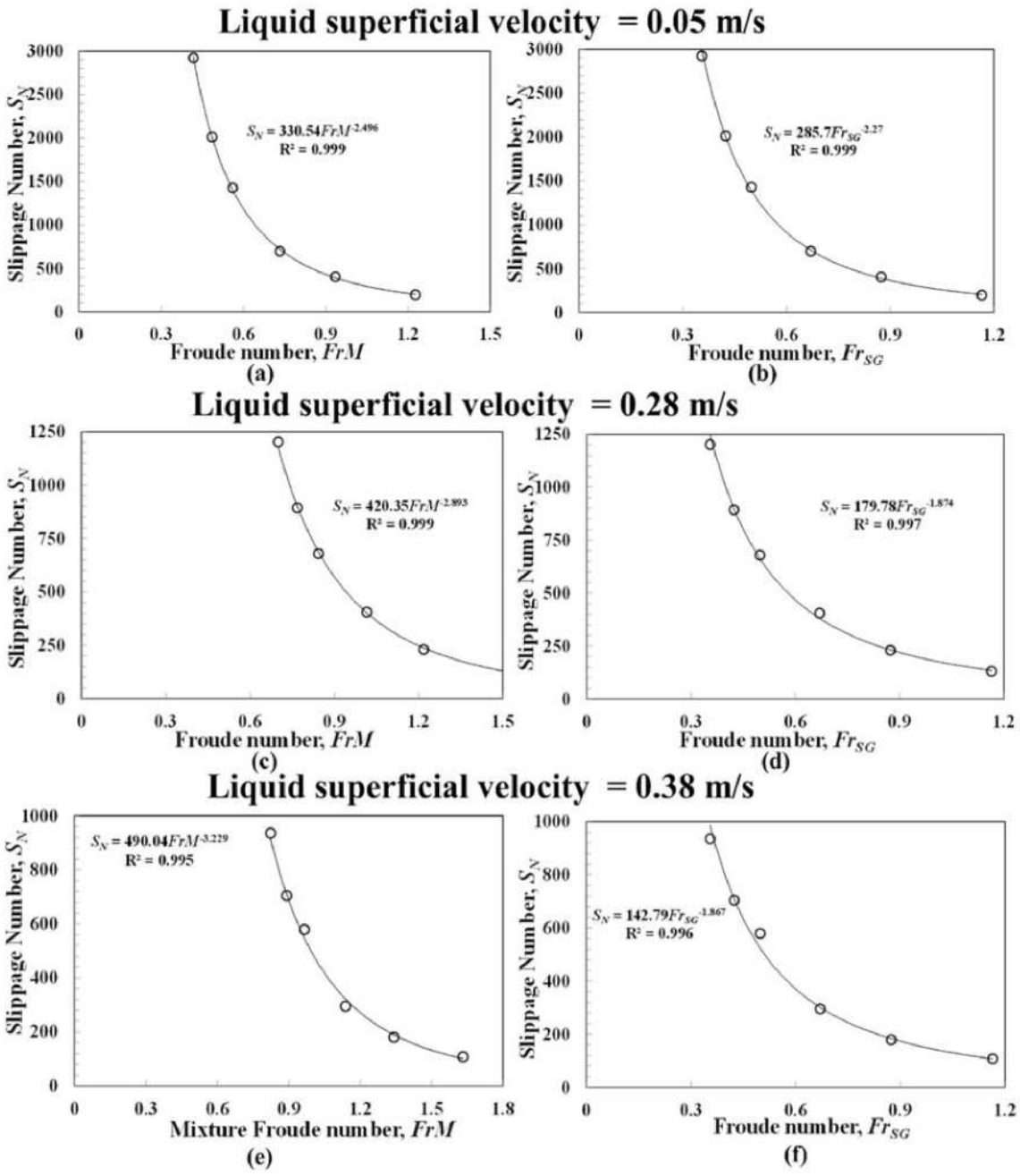

Figure 15. Correlation of Slippage Number (S_N) with either Froude Number (Fr_{SG}) or Mixture Froude Number (FrM) for upward flows. System fluid: air–silicone oil. Flow pattern under consideration: Slug flow. Liquid superficial velocity of (**a**) 0.05 m/s, (**b**) 0.05 m/s, (**c**) 0.28 m/s, (**d**) 0.28 m/s, (**e**) 0.38 m/s, and (**f**) 0.38 m/s.

Figure 15 shows a significantly large S_N which, is provoked by a large difference between the homogeneous mixture density and the two-phase flow mixture density. This large difference is based on the significant slippage between the liquid and gas phases.

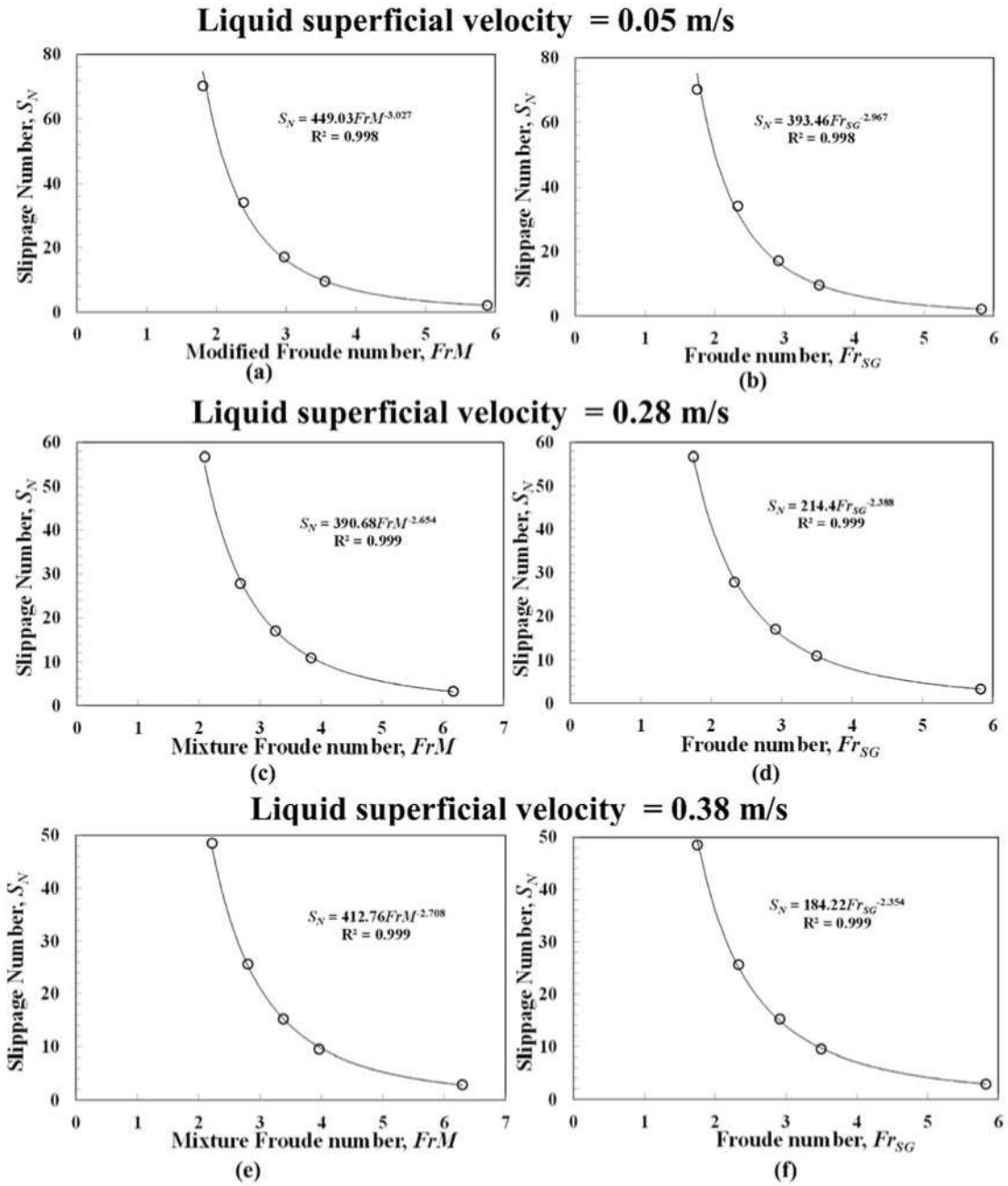

Figure 16. Correlation of Slippage Number (S_N) with either Froude Number (Fr_{SG}) or Mixture Froude number (FrM) for upward flows. System fluid: air–silicone oil. Flow pattern under consideration: Churn flow. Liquid superficial velocity of (**a**) 0.05 m/s, (**b**) 0.05 m/s, (**c**) 0.28 m/s, (**d**) 0.28 m/s, (**e**) 0.38 m/s, and (**f**) 0.38 m/s.

The figure also shows that there is a vast difference between the observed plots of S_N versus FrM and S_N versus Fr_{SG}, as shown through the correlations obtained through curve fitting. Thus, this shows that the assumption that U_{SG} can be used to replace U_m is not valid in this case. On the other hand, Figure 16 depicts churn flow, which occurs at a relatively higher gas superficial velocities than in slug flow. As expected, the slippage between the liquid and gas phases is smaller than that of slippage in the slug flow regime.

As a consequence, the disparity between the two densities is lower, and hence the S_N is also lower.

A comparable observation, seen in Figure 15, is also observed here, in Figure 16. Figure 16 displays a noteworthy variance between the experimental plots of S_N versus *FrM* and S_N versus Fr_{SG} using the correlations obtained through curve fitting. Thus, the assumption that U_{SG} can be used as a replacement for U_m is also not valid in this case.

It can be concluded, therefore, that the assumption of U_{SG} is approximately equal to U_m is strongly dependent on the range of values of U_{SG}/U_m and void fraction.

4.6. Zuber and Findlay's Proposed Drift-Flux Model Approach

The Zuber and Findlay [45]'s drift–flux model was employed in this work to correlate the actual gas velocity, V_G, and the mixture velocity, U_m, utilizing the two drift–flux variables, C_0 and U_{gd} and is of the following form:

$$V_G = \frac{U_{SG}}{\varepsilon_G} = C_0 U_m + U_{gd} \tag{25}$$

where, V_G, C_0, U_m, and U_{gd} are the actual gas velocity averaged across the pipe area, distribution coefficient describing the influence of velocity and concentration attributes within the two-phase fluid mixture, the mixture velocity, and the drift velocity of the gas describing the buoyancy effect, respectively.

According to the model presented in Equation (25), the values of C_0 and U_{gd} are obtained from a graph of V_G against the U_m for the upward and downward flows. C_0 is the line gradient from the plot, while U_{gd} is the intercept on the *y*-axis. Observation from Figure 17a,b shows that a straight-line relationship is confirmed between V_G and U_m for both the downward and upward flows, as suggested in [45] and endorsed by several investigators. The values of C_0 and U_{gd} are 1.03 and 0.14 m/s and 1.00 and 0.37 m/s, respectively, obtained from the downward and upward flows plot. The justification for the observed trend can be explained by considering the phase concentration attributes in upward churn and annular flows and downward annular flows. The overall gas distribution is consistent in the upward churn flow because of the appearance of some droplets entrained uniformly within the gas matrix, and consequently, C_0 is approximately equal to one. Similarly, in upward or downward annular flows, where liquid moves upward or downward partially in the semblance of entrained droplets of liquid in the gas matrix and as a thin film on the pipe walls, C_0 is also approximately equal to one since the non-uniform effects are growing strong. Therefore, a conclusion can be that the C_0 of upward flows is slightly lower than that of downward flows.

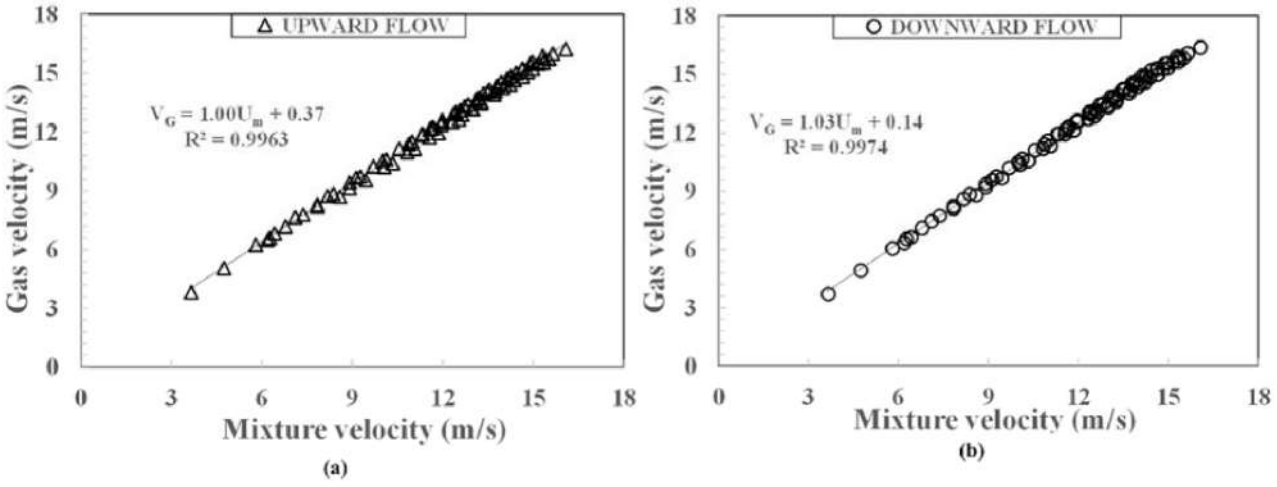

Figure 17. The relationship between the actual gas velocity and mixture velocity for the (**a**) upward and (**b**) downward flows.

Different values of C_0 and U_{gd} are obtained by linearly fitting the plot of V_G versus U_m at a range of liquid superficial velocity of 0.02 to 0.2 m/s for the upward and downward flows. Table 4 and Figures 18 and 19 shows the concluding results.

Table 4. Distribution coefficient (C_0) and drift velocity (U_{gd}) for the upward and downward flows.

	Upward Flows		Downward Flows	
U_{SL} (m/s)	C_0	U_{gd} (m/s)	C_0	U_{gd} (m/s)
0.02	1.0006	0.160	1.0160	0.0650
0.04	1.0010	0.260	1.0250	0.0690
0.08	1.0080	0.460	1.0340	0.1330
0.1	1.0220	0.280	1.0470	0.0260
0.2	1.0330	0.130	1.0650	−0.130

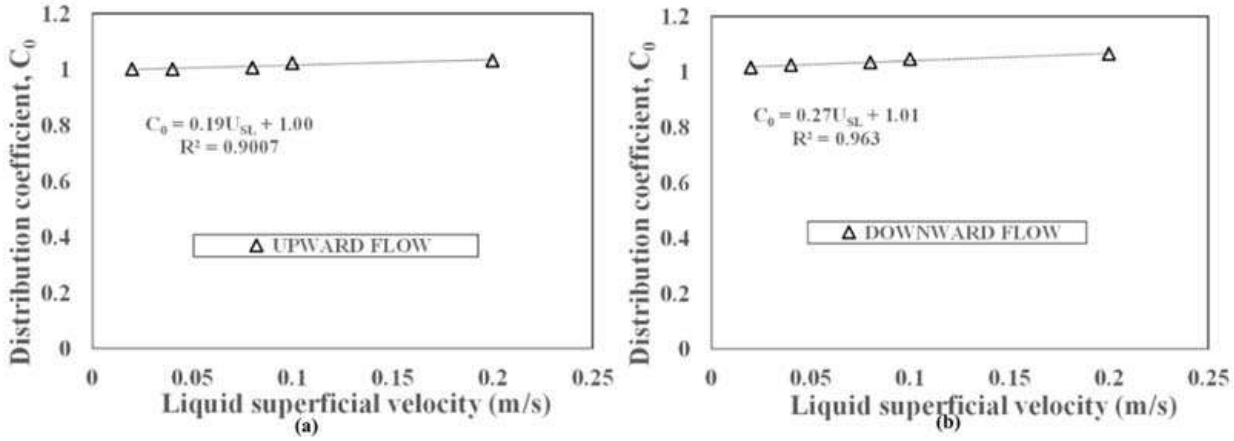

Figure 18. Distribution coefficient versus liquid superficial velocity for both (**a**) upward and (**b**) downward flows.

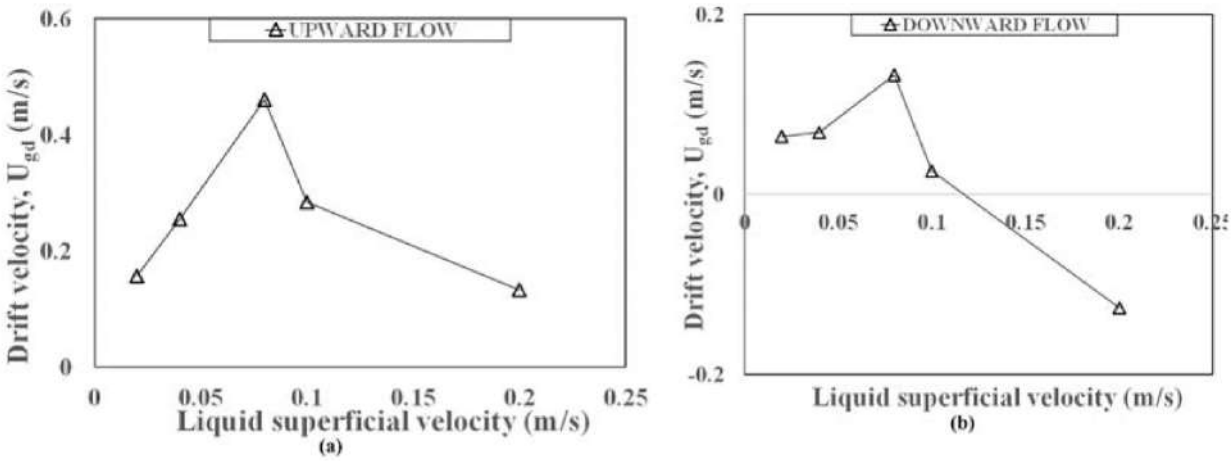

Figure 19. Drift velocity, U_{gd}, for the (**a**) upward and (**b**) downward flows.

Additionally, a plot of C_0against U_{SL} reveals that increasing liquid superficial velocity is associated with a corresponding linear increase of C_0 value for both downward and upward flows. A linear correlation is established between C_0 and U_{SL}.

Figure 19 shows that the drift velocity (U_{gd}) initially increases linearly with liquid superficial velocities of 0.02 to 0.08 m/s, then decreases linearly at liquid superficial velocities greater than 0.08 m/s. The initial increase in the drift velocity results from the higher gas buoyant force playing on the gas phase average flow pathway. By increasing the liquid superficial velocity from 0.1 to 0.2 m/s, the gas phase moves in the pathway

of average flow and, as a result, the liquid phase moves faster than the gas phase. It is accountable for the seen drop in U_{gd} for the upward and downward flows.

As noted by Bhagwat and Ghajar [1] and confirmed in this work, the U_{gd} for the upward and downward flows at a liquid superficial velocity of 0.2 m/s displayed in Table 4 may be applied reciprocally by exchanging the sign of the U_{gd} from plus to minus with the assumption that direction of flow of the phase velocities is positive.

4.7. Performance Investigation of Empirical Correlations for Estimating Void Fraction

The performance of ten selected void fraction correlations was analysed to find the one that can accurately predict void fraction for downward and upward flows. The ten considered correlations include [14,25,46–52]. The Root Mean Square Error (RMSE) was used to analyse the performance of these correlations.

$$RMSE = \sqrt{\frac{1}{N-1}\sum_{i=1}^{N}\left(\frac{(1-H_L)_{predicted}-(1-H_L)_{measured}}{(1-H_L)_{measured}}\right)^2} \times 100 \quad (26)$$

where: N denotes the number of data points analysed and $1 - H_L$ is the void fraction.

Figure 20 reveals that, for the upward flow, the most outstanding performing correlations whose RMSE is not above 4% include: Dix [14,47,52]'s. While for the downward flows, the most striking correlations whose RMSE is also not above 4% include Usui and Sato [14] and [Woldesemayat and Ghajar [52]. It can be concluded, therefore, that the [14] correlation based on RMSE is the most outstanding performing correlation for estimating the void fraction for the flows in the upward and downward configurations.

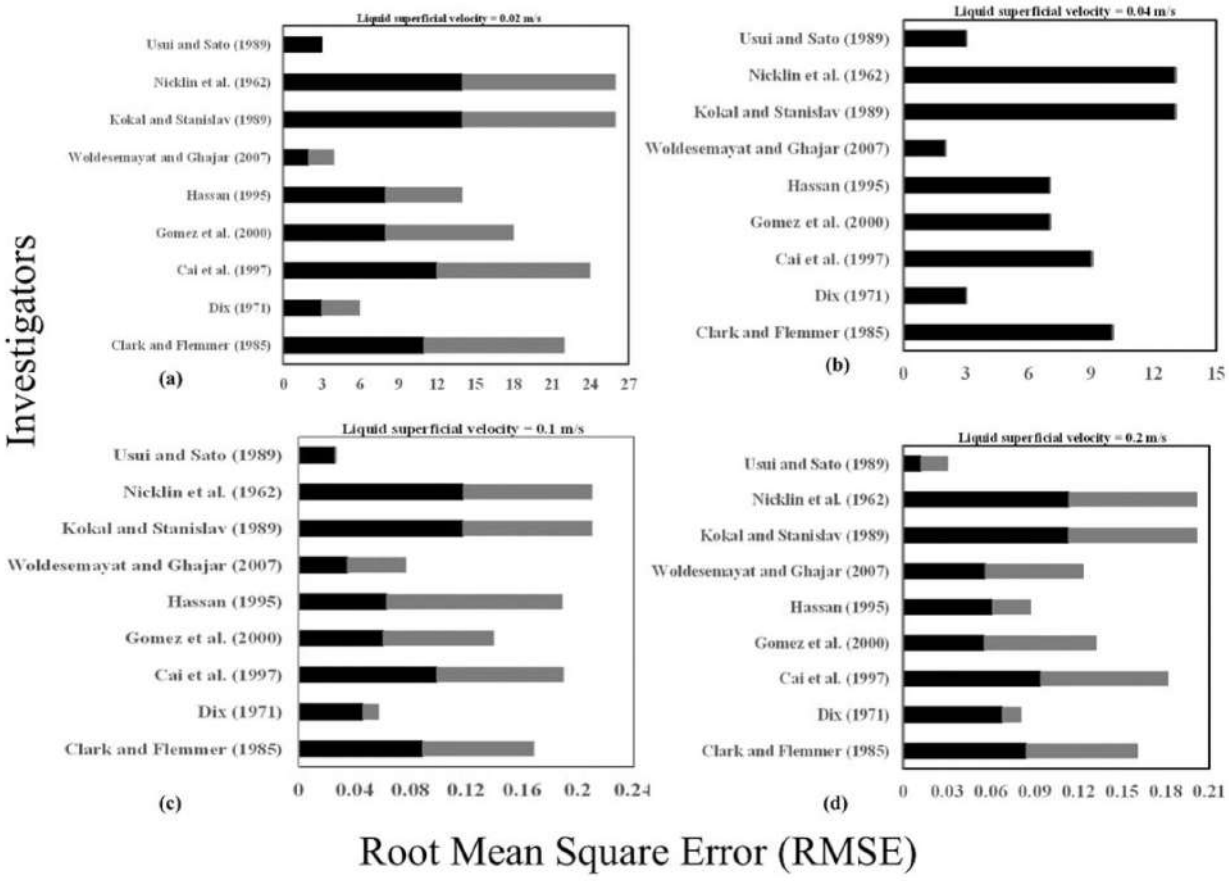

Figure 20. The calculated Root Mean Square Error (RMSE) from the 10 selected void fraction correlations at liquid superficial velocity of: (**a**) 0.02 m/s (**b**) 0.04 m/s (**c**) 0.1 m/s and (**d**) 0.2 m/s. The black bars represent the RSME values in the upward flow, while the RSME values for the downward flow are symbolized by the grey bars.

5. Conclusions

To understand the gap in the knowledge on liquid fraction behaviour in large diameter pipes concerned with upward and downward flows, the present work undertook experimental research with air and water in pipes of 127 mm internal diameter. The liquid fraction was measured using advanced conductance ring probes. To accomplish the goals of the current work, the investigated parameters are PDF, PSD, S_N, C_0, and U_{gd}. The examination of the air–water flow characteristics and behaviour for the upward (85 cases) and downward (85 cases) flows draw the following conclusions:

- The flow patterns encountered in the upward flow are churn and annular flows whereas, annular flow was seen in the downward flow scenario at the same flow conditions.
- The matching of the present work against the published Godbole et al. [42] (upward flow) and Bhagwat and Ghajar [1] (downward flow) void fraction data revealed the same tendency.
- The average liquid fractions obtained at low gas superficial velocities for the upward flow were seen to be considerably higher than those for the downward flow.
- An excellent relationship was established between the S_N and FrM for the two pipe configurations. The assumption that U_{SG} is approximately equal to U_m is strongly dependent on the range of values of U_{SG}/U_m and void fraction.
- The S_N values for the upward and downward flows at higher values of mixture Froude number are nearly equal, showing that both the gas and liquid flow together as a homogeneous mixture.
- In support of the conclusions of Al-Sarkhi et al. [44], the S_N can be employed as a swift flow regime discerning procedure.
- The C_0 of the upward flow is lower than it is in the downward flow. The U_{gd} for the upward flow, on the other hand, was discovered to be larger than that it was in the downward flow.
- An excellent relationship was observed between the C_0 and liquid superficial for the two pipe configurations.
- The correlation suggested in Usui and Sato [14] for estimating void fraction for the two pipe configurations was the most outstanding performing correlation based on the Root Mean Square Error (RMSE), less than 4% for all scenarios investigated.

Author Contributions: M.A., Conceptualization, Experimentation, Writing–original draft preparation. O.T.K., Conceptualization, Writing-review and editing. F.O.O., Analysis, Conceptualization and Writing. D.O.U., Writing-review and editing. D.Z., Writing—review and editing. A.M.A., Writing-review and editing. A.A.-S., Writing—review and editing. All authors have read and agreed to the published version of the manuscript.

Funding: This research received no external funding.

Conflicts of Interest: The authors declare no conflict of interest.

References

1. Bhagwat, S.M.; Ghajar, A.J. Similarities and differences in the flow patterns and void fraction in vertical upward and downward two-phase flow. *Exp. Therm. Fluid Sci.* **2012**, *39*, 213–227. [CrossRef]
2. Wang, K.; Bai, B.; Cui, J.; Ma, W. A physical model for huge wave movement in gas–liquid churn flow. *Chem. Eng. Sci.* **2012**, *79*, 19–28. [CrossRef]
3. Waltrich, P.J.; Falcone, G.; Barbosa, J.R. Axial development of annular, churn and slug flows in a vertical tube. *Int. J. Multiph. Flow* **2013**, *57*, 38–48. [CrossRef]
4. Abdulkadir, M.; Mbalisigwe, U.P.; Zhao, D.; Hernandez-Perez, V.; Azzopardi, B.J.; Tahir, S. ; Tahir, S. Characteristics of churn and annular flows in a large diameter vertical riser. *Int. J. Multiph. Flow* **2019**, *113*, 250–263. [CrossRef]
5. Omebere-Iyari, N.K.; Azzopardi, B.J. A study of flow patterns for gas/liquid flow in small diameter tubes. *Chem. Eng. Res. Des.* **2007**, *85*, 180–192. [CrossRef]
6. Van der Meulen, G.P. Churn–Annular Gas–Liquid Flows in Large Diameter Vertical Pipes. Ph.D. Thesis, University of Nottingham, Nottingham, UK, 2012.

7. Schlegel, J.P.; Hibiki, T. A correlation for interfacial area concentration in high void fraction flows in large diameter channels. *Chem. Eng. Sci.* **2015**, *131*, 172–186. [CrossRef]
8. Almabrok, A.A.; Aliyu, A.M.; Lao, L.; Yeung, H. Gas–liquid flow behaviour in a downward section of large diameter vertical serpentine pipes. *Int. J. Multiph. Flow* **2016**, *78*, 25–43. [CrossRef]
9. Capovilla, M.S.; Coutinho, R.P.; de Sousa, P.C.; Waltrich, P.J. Experimental investigation of upward vertical two-phase high-velocity flows in large diameter pipes. *Exp. Therm. Fluid Sci.* **2019**, *102*, 493–505. [CrossRef]
10. Lokanathan, M.; Hibiki, T. Flow regime transition criteria for co-current downward two-phase flows in a vertical narrow rectangular channel. *Prog. Nucl. Energy* **2018**, *103*, 165–175. [CrossRef]
11. Bouyahiaoui, H.; Azzi, A.; Zeghloul, A.; Hassan, A.H.; Berrouk, A.S. Experimental investigation of vertically downward two-phase air–water slug flow. *J. Pet. Sci. Eng.* **2018**, *162*, 12–21. [CrossRef]
12. Wang, G.; Dang, Z.; Ju, P.; Yang, X.; Ishii, M.; Ireland, A.; Bajorek, S.; Bernard, M. Experimental study on interfacial structure and interfacial area transport in downward two-phase flow. *Int. J. Heat Mass Transf.* **2016**, *106*, 1303–1317. [CrossRef]
13. Wang, G.; Li, Z.; Yousaf, M.; Yang, X.; Ishii, M. Experimental study on vertical downward air–water two-phase flow in a large diameter pipe. *Int. J. Heat Mass Transf.* **2018**, *118*, 919–930. [CrossRef]
14. Usui, K.; Sato, K. Vertically downward two-phase flow (1) void distribution and average void fraction. *J. Nucl. Sci. Technol.* **1989**, *26*, 670–680. [CrossRef]
15. Dang, Z.; Wang, G.; Ju, P.; Yang, X.; Bean, R.; Ishii, M.; Bajorek, S.; Bernard, M. Experimental study of interfacial characteristics of vertical upward air–water two-phase flow in 25.4 mm ID round pipe. *Int. J. Heat Mass Transf.* **2017**, *108*, 1825–1838. [CrossRef]
16. Abdulkadir, M.; Zhao, D.; Azzi, A.; Lowndes, I.S.; Azzopardi, B.J. Two-phase air–water flow through a large diameter vertical 180° return bend. *Chem. Eng. Sci.* **2012**, *79*, 138–152. [CrossRef]
17. Bouyahiaoui, H.; Azzi, A.; Zeghloul, A.; Hassan, A.H.; Al-Sarkhi, A.; Parsi, M. Vertical upward and downward churn flow: Similarities and differences. *J. Nat. Gas Sci. Eng.* **2020**, *73*, 103080. [CrossRef]
18. Tian, D.; Yan, C.; Sun, L.; Tong, P.; Liu, G. Comparison of local interfacial characteristics between vertical upward and downward two-phase flows using a four-sensor optical probe. *Int. J. Heat Mass Transf.* **2014**, *77*, 1183–1196. [CrossRef]
19. Chalgeri, V.S.; Jeong, J.H. Flow patterns of vertically upward and downward air–water two-phase flow in a narrow rectangular channel. *Int. J. Heat Mass Transf.* **2019**, *128*, 934–953. [CrossRef]
20. Golan, L.P.; Stenning, A.H. Two-phase vertical flow maps. *Proc. Inst. Mech. Eng.* **1969**, *14*, 108–114. [CrossRef]
21. Beggs, H.D. An Experimental Study of Two-Phase Flow in Inclined Pipes. Ph.D. Thesis, The University of Tulsa, Tulsa, OK, USA, 1972.
22. Oshinowo, T.; Charles, M.E. Vertical two-phase flow—Part 1: Flow pattern correlations. *Can. J. Chem. Eng.* **1974**, *52*, 25–35. [CrossRef]
23. Nguyen, V.T. Two Phase Gas–Liquid Concurrent Flow: An Investigation of Holdup, Pressure Drop and Flow Patterns in a Pipe at Various Inclinations. Ph.D. Thesis, The University of Auckland, Auckland, New Zealand, 1975.
24. Mukherjee, H. An Experimental Study of Inclined Two-Phase Flow. Ph.D. Thesis, The University of Tulsa, Tulsa, OK, USA, 1979.
25. Clark, N.N.; Flemmer, R.L. Predicting the holdup in two-phase bubble upflow and downflow using the Zuber and Findlay drift flux model. *AIChE* **1985**, *31*, 500–503. [CrossRef]
26. Jiang, Y. Void Fraction Measurements in Vertical Co-Current Upward and Downward Two-Phase Gas–Liquid Flow Using Densitometer. Master's Thesis, University of Saskatchewan, Saskatoon, SK, Canada, 1992.
27. Jiang, Y.; Rezkallah, K.S. A study on void fraction in vertical co-current upward and downward two-phase gas–liquid flow-II: Correlations. *Chem. Eng. Commun.* **1993**, *126*, 245–259. [CrossRef]
28. Sun, X.D.; Paranjare, S.; Kim, S.; Ozar, B.; Ishii, M. Liquid velocity in upward and downward air–water flows. *Annu. Nucl. Energy* **2004**, *31*, 357–373. [CrossRef]
29. Lee, J.Y.; Ishii, M.; Kim, N.S. Instantaneous and objective flow regime identification method for the vertical upward and downward co-current two-phase flow. *Int. J. Heat Mass Transf.* **2008**, *51*, 3442–3459. [CrossRef]
30. Abdulkadir, M.; Hernandez–Perez, V.; Kwatia, C.A.; Azzopardi, B.J. Interrogating flow development and phase distribution in vertical and horizontal pipes using advanced instrumentation. *Chem. Eng. Sci.* **2018**, *186*, 152–167. [CrossRef]
31. Abdulkadir, M.; Jatto, D.G.; Abdulkareem, L.A.; Zhao, D. Pressure drop, void fraction and flow pattern of vertical air–silicone oil flows using differential pressure transducer and advanced instrumentation. *Chem. Eng. Res. Des.* **2020**, *159*, 262–277. [CrossRef]
32. Omebere-Iyari, N.K. The Effect of Pipe Diameter and Pressure in Vertical Two-Phase Flow. Ph.D. Thesis, University of Nottingham, Nottingham, UK, 2006.
33. Van der Meulen, G.P.; Zangana, M.; Zhao, D.; Azzopardi, B.J. Phase distribution measurements by conductance probes and pressure drop in gas-liquid flows. In Proceedings of the ExHFT-7, Krakow, Poland, 28 June–30 July 2009.
34. Zangana, M. Film Behaviour of Vertical Gas-Liquid Flow in a Large Diameter Pipe. Ph.D. Thesis, University of Nottingham, Nottingham, UK, 2011.
35. Abdulkadir, M. Experimental and Computational Fluid Dynamics (CFD) Studies of Gas-Liquid Flow in Bends. Ph.D. Thesis, University of Nottingham, Nottingham, UK, 2011.
36. Sharaf, S.; van der Meulen, G.P.; Agunlejika, E.O.; Azzopardi, B.J. Structures in gas–liquid churn flow in a large diameter vertical pipe. *Int. J. Multiph. Flow* **2016**, *78*, 88–103. [CrossRef]

37. Abdulkadir, M.; Hernandez-Perez, V.; Lowndes, I.S.; Azzopardi, B.J.; Brantson, E.T. Detailed analysis of phase distributions in a vertical riser using wire mesh sensor (WMS). *Exp. Therm. Fluid Sci* **2014**, *59*, 32–42. [CrossRef]
38. Fossa, M. Design and performance of a conductance probe for measuring the liquid fraction in two-phase gas–liquid flows. *Flow Meas. Instrum.* **1998**, *9*, 103–109. [CrossRef]
39. Pereyra, E.; Torres, C. *FLOPATN—Flow Pattern Prediction and Plotting Computer Code*; The University of Tulsa: Tulsa, OK, USA, 2005.
40. Taitel, Y.; Barnea, D.; Dukler, A.E. Modelling flow pattern transitions for steady upward gas-liquid flow in vertical tubes. *AIChE J.* **1980**, *26*, 345–354. [CrossRef]
41. Jayanti, S.; Hewitt, G.F. Prediction of the slug-to-churn flow transition in vertical two-phase flow. *Int. J. Multiph. Flow* **1992**, *18*, 847–860. [CrossRef]
42. Godbole, P.V.; Tang, C.C.; Ghajar, A.J. Comparison of Void Fraction Correlations for Different Flow Patterns in Upward Vertical Two-Phase Flow. *Heat Transf. Eng.* **2011**, *32*, 843–860. [CrossRef]
43. Costigan, G.; Whalley, P.B. Slug flow regime identification from dynamic void fraction measurements in vertical air–water flows. *Int. J. Multiph. Flow* **1997**, *23*, 263–282. [CrossRef]
44. Al-Sarkhi, A.; Cem, S.; Eduardo, P. New dimensionless number for gas–liquid flow in pipes. *Int. J. Multiph. Flow* **2016**, *81*, 15–19.
45. Zuber, N.; Findlay, J.A. Average volumetric concentration in two-phase flow systems. *J. Heat Transf.* **1965**, *87*, 453–468. [CrossRef]
46. Nicklin, D.J.; Wilkes, J.O.; Davidson, J.F. Two-phase flow in vertical tubes. *Trans. Inst. Chem. Eng.* **1962**, *156*, 61–68.
47. Dix, G.E. Vapour Void Fractions for Forced Convection with Sub Cooled Boiling at Low Flow Rates. Ph.D. Thesis, University of California, Berkeley, CA, USA, 1971.
48. Kokal, S.L.; Stanislav, J.F. An experimental study of two phase flow in slightly inclined pipes II: Liquid holdup and pressure drop. *Chem. Eng. Sci.* **1989**, *44*, 681–693. [CrossRef]
49. Hasan, A.R. Void fraction in bubbly and slug flow in downward vertical and inclined systems. *Soc. Pet. Eng. Prod. Facil.* **1995**, *10*, 172–176. [CrossRef]
50. Cai, J.; Chen, T.; Ye, Q. Void fraction in bubbly and slug flow in downward air–oil two phase flow in vertical tubes. In Proceedings of the International Symposium on Multiphase Flow, Beijing, China, 7–11 October 1997.
51. Gomez, L.E.; Shoham, O.; Schmidt, Z.; Chokshi, R.N.; Northug, T. Unified mechanistic model for steady-state two-phase flow: Horizontal to vertical upward flow. *Soc. Pet. Eng. J.* **2000**, *5*, 339–350. [CrossRef]
52. Woldesemayat, M.A.; Ghajar, A.J. Comparison of void fraction correlations for different flow patterns in horizontal and upward inclined pipes. *Int. J. Multiph. Flow* **2007**, *33*, 347–370. [CrossRef]